Effective potential and chiral symmetry breaking

David Hochberg*
Centro de Astrobiología, CSIC–INTA, Carretera Ajalvir Kilómetro 4, 28850 Torrejón de Ardoz, Madrid, Spain
(Received 7 July 2009; published 20 January 2010)

The nonequilibrium effective potential is calculated for the Frank model of spontaneous mirror-symmetry breaking in chemistry in which external noise is introduced to account for random environmental effects. The well-mixed limit, corresponding to negligible diffusion, and the case of diffusion in two space dimensions are studied in detail. White noise has a disordering effect in the former case, whereas in the latter case a phase transition occurs for external noise exceeding a critical intensity which racemizes the system.

DOI: 10.1103/PhysRevE.81.016106 PACS number(s): 82.20.−w, 05.40.Ca, 11.30.Qc, 87.15.B−

I. INTRODUCTION

In chemistry, enantiomers are molecules that are nonsuperimposible complete mirror images of each other. A remarkable feature of nature is that this mirror or chiral symmetry is broken in all biological systems, where processes crucial for life such as replication, imply chiral supramolecular structures, sharing the same chiral sign (homochirality) for all present living systems as we know them. These chiral structures are proteins, composed by amino acids almost exclusively found as the left-handed enantiomers (L), DNA, RNA polymers and sugars with chiral building blocks composed by right-handed (D) monocarbohydrates, and chiral amphiphiles that form membranes. This fact has led to the widespread perception that the presence of handed or chiral molecules is a unique signature of living systems. The emergence of this biological homochirality in the chemical evolution from prebiotic to living systems is a tantalizing enigma in the origin of life as is the robustness of homochirality in actual living systems. Current reviews and surveys of the origin of homochirality can be found in [1–6]. Previous hypotheses suggesting that homochirality emerged after the development of the primeval biological system [7] are being replaced by the widespread conviction that enantiomerically pure compounds are a prerequisite for the evolution of living species and that mirror-symmetry breaking must have taken place before the emergence of life [8–10].

The key ingredients of theoretical models of mirror-symmetry breaking processes in chemistry [11] include reactions in which the chiral products serve as catalysts to produce more of themselves while inhibiting the production of their enantiomer or mirror-image counterparts. Frank's original model [12–18], a variant of which we study here [19] (see Sec II), involves the autocatalysis of the two enantiomers, denoted herewith as L and D and mutual inhibition or antagonistic effects between the two chiral species. This mutual inhibition occurs through the formation of LD heterodimers that are removed from the reacting system. More intricate and complex polymerization networks that lead to populations of chiral oligomers can be elaborated [21–24] on the basis of the fundamental Frank paradigm. In these polymerization models, the crucial chiral antagonism occurs through enantiomeric cross inhibition. Motivated by recent experimental results indicating that mechanical stirring [25,26] can effectively bias the chirality as well as numerical studies on the effects of turbulent advection velocities [22], Gleiser and co-workers have been examining the influence that external ambient noise can have on mirror-symmetry breaking in specific models of chiral polymerization [27]. The above are examples of external noises to be distinguished from noises inherent to the chemical system, such as epimerization, reaction or diffusion noise, or temperature fluctuations. The latter are examples of multiplicative noise, in which the chemical concentrations [28] or kinetic rate constants would fluctuate [29], respectively. The noise considered by Gleiser *et al.* is taken to model environmental disturbances present in early prebiotic planetary scenarios. For example, the noise amplitude could represent sudden increases in the pressure due to meteor impacts or volcanic eruptions. They find the important result that white noise has a racemizing tendency and can thus wipe out any net value of the enantiomeric excess.

The evidence for the noise-induced chiral symmetry restoration reported in [27] is based on direct numerical simulation. Symmetry breaking phenomena in nonequilibrium stochastic systems can be treated as well by *analytic* means which afford complementary perspectives on the problem and underscore the deep formal analogies between stochastic and quantum physics. The addition of noise to the chemical kinetic equations converts these into Langevin equations. Considerable information and physical insight can be gained from studying such types of stochastic equations. With this purpose in mind, some years ago we considered classical field theories subject to additive noise $\xi(\boldsymbol{x},t)$ described by equations of the form

$$\mathcal{D}\phi(\boldsymbol{x},t) = F[\phi(\boldsymbol{x},t)] + \xi(\boldsymbol{x},t), \tag{1}$$

where $\mathcal{D}$ is any linear differential operator involving arbitrary time and space derivatives, but that does not explicitly involve the stochastic field ϕ. The function F is an arbitrary forcing term, generally nonlinear in the field ϕ.

These stochastic partial differential equations (SPDEs) can then be studied using a functional-integral formalism [30] which makes manifest the deep connections between quantum field theory (QFT) and nonequilibrium fluctuation phenomena. We demonstrated that if the noise is Gaussian

*hochbergd@inta.es

and translation invariant, we can always split the noise two-point function into an amplitude $\mathcal{A}$ and shape function g_2 and this correlation can be expressed as

$$\langle \xi(\boldsymbol{x},t)\xi(\boldsymbol{x}',t')\rangle = \mathcal{A}g_2(x-x'), \tag{2}$$

with the convention that

$$\int d^d\boldsymbol{x}dtg_2^{-1}(\boldsymbol{x},t) = 1 = g_2^{-1}(\boldsymbol{k}=0,\ \ \omega=0). \tag{3}$$

Here, $\boldsymbol{k}$ and ω denote the wave number and frequency, respectively. Then a one-loop field-theoretic effective potential $\mathcal{V}$ can be calculated which is associated to the original SPDE Eq. (1) and which bears close resemblance to the one-loop effective potential for scalar QFT. The effective potential simply means a function which agrees with the classical potential at lowest-order perturbation theory, but which is modified in higher orders by stochastic corrections, that is, by the noise. Such potential functions can be calculated with the help of field theory in which systems are treated as a continuum and "one-loop" means an expansion to first order in the noise strength $\mathcal{A}$.

The one-loop effective potential for homogeneous and static fields in any dimension d is given by [30,31]

$$\mathcal{V}[\phi] = \frac{1}{2}F^2[\phi] + \frac{1}{2}\mathcal{A}\int \frac{d^d\boldsymbol{k}d\omega}{(2\pi)^{d+1}} \times \ln\left[1 + \frac{\tilde{g}_2(\boldsymbol{k},\omega)F[\phi]\delta^2F/\delta\phi\delta\phi}{(\mathcal{D}^\dagger(\boldsymbol{k},\omega) - \delta F^\dagger/\delta\phi)(\mathcal{D}(\boldsymbol{k},\omega) - \delta F/\delta\phi)}\right] - (\phi\to\phi_0) + O(\mathcal{A}^2). \tag{4}$$

Here, ϕ_0 is any convenient background field. In the absence of symmetry breaking, it is most convenient to choose $\phi_0=0$. As discussed in [30], Eq. (4) is qualitatively similar to the one-loop effective potential in self-interacting scalar quantum field theory [32,33]. The potential $\mathcal{V}$ has a deep physical meaning and inherits many of the physical features and information content of the potential associated with QFTs. It is also extremely useful for obtaining the effective *deterministic* equations of motion at one-loop order obeyed by the dynamical field variables. Indeed, from Eq. (4), we see that $\mathcal{V}$ is proportional to the square of the forcing term F appearing in the original SPDE, Eq. (1). Hence, the square root $(2\mathcal{V})^{1/2}$ yields an effective force $F_{\mathcal{A}}$ and minus the integral of this effective force will yield the effective "mechanical" potential $V_{\mathcal{A}}=-\int F_{\mathcal{A}}$, whereby all these physical quantities are calculable by means of a loop expansion in the noise amplitude $\mathcal{A}$. To avoid confusion, we will distinguish this mechanical potential V from the higher-level field-theoretic potential $\mathcal{V}$. The logical sequence of steps is summarized schematically in Eq. (5), indicating the route leading from the stochastic differential equation to the effective mechanical potential

$$\text{SPDE} \Rightarrow \mathcal{V} \Rightarrow F_{\mathcal{A}} = (2\mathcal{V})^{1/2} \Rightarrow V_{\mathcal{A}} = -\int F_{\mathcal{A}}. \tag{5}$$

The purpose of this paper is to provide a quantitative understanding of the impact of external noise and chiral bias on spontaneous mirror-symmetry breaking (SMSB) processes in chemistry as an important application of the formal methods developed in [30,31]. We therefore calculate the potential $V_{\mathcal{A}}$ for the Frank model, as this serves as the starting point for many other more complex models of mirror-symmetry breaking. The relative minima (maxima) of $V_{\mathcal{A}}$ correspond to the asymptotically stable (unstable) final states of the reacting system. Noise alters the form of the potential and hence affects the corresponding stability properties of the underlying chemical reactions.

This paper is organized as follows. In Sec. II A, we introduce the reaction steps that define the open flow Frank model and derive the tree-level (in the absence of noise) potential V in the adiabatic regime where the total net chiral matter is approximately constant. The direct production of enantiomers tends to racemize the system, that is, destabilizes the symmetric pair of chiral minima. Over abundant monomer production will fully racemize the system. The effect of chiral bias is considered next in Sec. II B. Bias leads to a tilted potential, one of the two chiral minima becomes an absolute minimum, and there is no racemic state. In Sec. III, we add white noise and derive the effective potential. In this zero-dimensional case, the noise has a disordering effect on the system and the chirality is degraded by the noise, but there is no transition to a racemic state, certainly not within the confines of the lowest-order perturbation theory employed here. Independent evidence for this disordering behavior is provided by a Fokker-Planck treatment of similar zero-dimensional systems. The joint effect of noise and bias is also considered. Spatially dependent noise and diffusion is treated in detail in Sec. IV and we derive the corresponding effective potential for $d=2$ dimensions in Sec. IV A. The field-theoretic potential $\mathcal{V}$ has a short-distance divergence and thus requires *renormalization* and will consequently depend on an arbitrary sliding scale μ [31]. This dependence is correctly handled through the renormalization-group (RG) equations, which imply that the Frank model parameters will run with this scale μ in a mathematically explicit way (Sec. IV B). This is achieved using RG-improved perturbation theory. We study the resultant scale-dependent mechanical potential $V_{\mathcal{A}}$ as a function of the competition between noise intensity and diffusion and consider some illustrative cases of relative physical length scales of observation in Sec. IV C. Increasing noise intensity leads to a chiral-racemic phase transition whenever the diffusion length scale is greater than the microscale at which the chemical reactions take place. The combined effects of noise and chiral bias are treated in Sec. IV D. Our results are discussed briefly in Sec. V and some integrals needed for the calculation of the potentials are listed in the Appendix.

II. FRANK MODEL POTENTIAL

A. Tree-level and no chiral bias

The reaction scheme we study here is composed of the following steps, where the $k_i(k_{-i})$ denote the forward (reverse) reaction-rate constants and A is an achiral reactant maintained at constant concentration by controlling its inflow to the system [20]:

Direct production of chiral monomers

$$A \underset{k_{-1}}{\overset{k_1}{\rightleftharpoons}} L, \quad A \underset{k_{-1}}{\overset{k_1}{\rightleftharpoons}} D. \tag{6}$$

Autocatalytic amplification

$$L + A \underset{k_{-2}}{\overset{k_2}{\rightleftharpoons}} L + L, \quad D + A \underset{k_{-2}}{\overset{k_2}{\rightleftharpoons}} D + D. \tag{7}$$

Mutual inhibition or heterodimerization

$$L + D \overset{k_3}{\rightarrow} LD. \tag{8}$$

We express the corresponding mean-field kinetic equations in terms of the enantiomeric excess $\eta=(L-D)/(L+D)$, which is the order parameter, and the total chiral matter $\chi=L+D$. From Eqs. (6)–(8), we thus obtain

$$\frac{d}{dt}\eta = -2k_1 A\frac{\eta}{\chi} + \frac{1}{2}(k_3 - k_{-2})\chi\eta(1-\eta^2), \tag{9}$$

$$\frac{d}{dt}\chi = 2k_1 A + (k_2 A - k_{-1})\chi - \chi^2\left[k_{-2} + \frac{1}{2}(k_3 - k_{-2})(1-\eta^2)\right]. \tag{10}$$

By taking into account the constant concentration of the achiral reactant A, we introduce dimensionless time $\tau=(k_2A-k_{-1})t$ and verify that when the rate of autocatalytic amplification exceeds the rate of monomer decay, χ changes more rapidly than the enantiomeric excess η. The system rapidly reaches a quasisteady state for $\chi(d\chi/dt\approx 0)$ and then the slow variable η evolves and the full system reaches its true steady state [34]. For this adiabatic regime, we then put $\chi\rightarrow\chi^*$ in Eq. (9), where χ^* denotes the quasisteady value for χ. Then define the potential V by

$$\frac{d\eta}{dt} = F(\eta) = -\frac{dV(\eta)}{d\eta} = -V'(\eta), \tag{11}$$

which implies

$$\frac{V(\eta)}{b} = \frac{\eta^4}{4} + \left(r - \frac{1}{2}\right)\eta^2 + v_0, \tag{12}$$

where v_0 is an integration constant, and where $b=\frac{1}{2}(k_3-k_{-2})\chi^*>0$, $r=a/b$, and $a=k_1A/\chi^*\geq 0$. For the scaled potential, r is the only free variable. This is plotted in Fig. 1 as a function of $-1\leq\eta\leq 1$ and for $0\leq r\leq\frac{1}{2}$. The absolute minima of V correspond to the asymptotic stable states of the chemical system and are located at $\eta=\pm\sqrt{1-2r}$. By varying r, we see how direct chiral monomer production $(k_1>0)$ tends to racemize the system as the two chiral minima move continuously toward zero and then coalesce at the origin as k_1A increases from zero. The dependence of η on r is displayed in Fig. 2. Strict homochirality $|\eta|=1$ holds only for $k_1A=0$, otherwise, $k_1A>0$ implies $|\eta|<1$. For $r\geq\frac{1}{2}$, the chiral-symmetric state $\eta=0$ is the only stable solution. Gleiser and Walker [27] obtained a potential qualitatively similar to Fig. 1, for a reduced $N=2$ polymerization model with direct production of monomers, which also clearly exhibits the racemizing tendency of such autogenic terms [see their Fig. 1(a)]. Their potential generalizes that obtained by Brandenburg and Multamäki [22], which contains quadratic and logarithmic terms; ours in Eq. (12) has instead quartic and quadratic terms. The explicit mathematical form of the potential is not so crucial; the true significance of the potential lies rather in its maxima or minima structure.

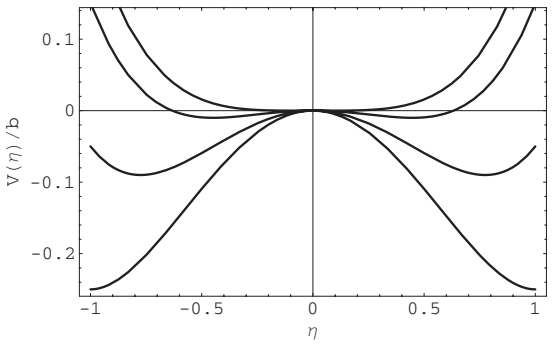

FIG. 1. The Frank model potential $V(\eta)/b$, Eq. (12), displaying the racemizing tendency of the direct chiral monomer production $A\rightarrow L$, $A\rightarrow D$. The sequence of curves from bottom to top corresponds to $r=0,0.2,0.4$ and $r=0.5$. For $r>0.5$, the racemic state is the unique stable final outcome.

B. Chiral bias

External magnetic, electric, and gravitational fields, hydrodynamic vortex motion, as well as polarized radiation can induce mirror-symmetry breaking [35]. Chiral bias can be studied via the potential by assigning chiral specific reaction rates [27,36,37] to the monomer production and autocatalysis steps and substituting the rate constants k_i by $k_i^L=k_i(1+\frac{1}{2}\epsilon)$ and $k_i^D=k_i(1-\frac{1}{2}\epsilon)$, where $k_i=(k_i^L+k_i^D)/2$. In this situation, we must modify the steps Eqs. (6) and (7) as follows:

Biased production of chiral monomers

$$A \underset{k_{-1}^L}{\overset{k_1^L}{\rightleftharpoons}} L, \quad A \underset{k_{-1}^D}{\overset{k_1^D}{\rightleftharpoons}} D. \tag{13}$$

Biased autocatalytic amplification

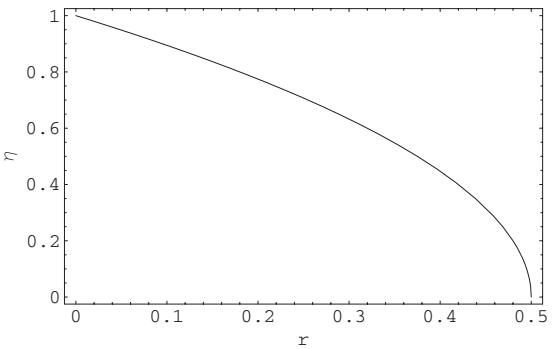

FIG. 2. Tree-level potential: the enantiomeric excess η as a function of $r=a/b$. We display the positive branch $\eta=+\sqrt{1-2r}$. There is also a mirror-image negative branch which completes the figure and gives the classic bifurcation diagram. Note $\eta=0$ for all $r>\frac{1}{2}$.

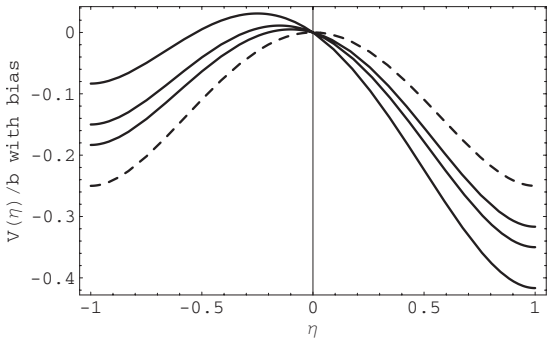

FIG. 3. Tree potential subject to small chiral bias, Eq. (17). The dashed curve corresponds to zero bias. For $\epsilon' > 0$, the point $\eta = 1$ is the absolute minimum of the potential. For the sequence of solid curves below dashed curve, from top to bottom, $\epsilon' = 0.1$, 0.2, and 0.5. For $\epsilon' < 0$, the curves will be tilted in the opposite sense.

$$L + A \underset{k_{-2}^{L}}{\overset{k_{2}^{L}}{\rightleftharpoons}} L + L, \quad D + A \underset{k_{-2}^{D}}{\overset{k_{2}^{D}}{\rightleftharpoons}} D + D. \tag{14}$$

Biased mean-field rate equations that generalize Eqs. (9) and (10) are straightforwardly derived from Eqs. (8), (13), and (14) and for the adiabatic regime $\chi \approx \chi^*$, we find the potential can be written as

$$V(\eta) = V_0(\eta) + \Delta V_\epsilon(\eta), \tag{15}$$

where V_0 denotes the unbiased $\epsilon = 0$ contribution and is given above in Eq. (12), whereas the biased part is

$$\Delta V_\epsilon(\eta) = -\frac{\epsilon}{2}\left[2k_1 A\frac{\eta}{\chi^*} + \left(k_2 A - k_{-1} - \frac{1}{2}k_{-2}\chi^*\right)\left(\eta - \frac{\eta^3}{3}\right)\right]. \tag{16}$$

For convenience, we now set $k_1 = 0$. Then we can factor out the overall scale factor b as we did above and express the biased potential as a function of a single free parameter $1 > \epsilon' \geq 0$,

$$\left(\frac{V(\eta)}{b}\right) = \frac{\eta^4}{4} - \frac{\eta^2}{2} - \epsilon'\left[\eta - \frac{\eta^3}{3}\right], \tag{17}$$

where $\epsilon' = \epsilon\frac{(k_2 A - k_{-1} - \frac{1}{2}k_{-2}\chi^*)}{(k_3 - k_{-2})\chi^*}$. We remark that for any nonzero bias $\epsilon > 0$ and in the *absence of any other influence*, there is no racemic solution. This is because the pure biased part of the potential Eq. (16) is an odd function of η, containing linear and cubic terms. Instead, a new unstable chiral solution emerges. There are then three chiral states, two are stable homochiral states located at $\eta = \pm 1$, together with this third unstable chiral, but not homochiral, state at $\eta = -\epsilon' < 0$ (see Fig. 3). For $\epsilon > 0$, the absolute minimum is located at $\eta = 1$ implying that the final outcome will be composed entirely of the L monomers. The above discussion applies equally well to the case where the bias parameter $\epsilon < 0$ is negative, in which case Fig. 3 is simply tilted in the opposite sense, with the D monomers being the favored stable outcome.

III. ADDING NOISE: THE WELL-MIXED CASE

In this section, we consider the effects of ambient white noise on well-mixed systems or equivalently, systems with zero or negligible diffusion. This association between mixing and diffusion becomes clear if we introduce the concept of mixing velocity u in a system on a length scale L. Then for a diffusion constant D, good mixing corresponds to large values of $\frac{uL}{D}$ and hence small values of D. In the absence of diffusion, the dynamics can be treated as zero dimensional. We are interested in the influence of a random external environment on the chemical system and the simplest way to consider this is by adding white noise to the kinetic rate equations. This is a working assumption in what follows. So, adding noise to Eq. (11) then leads to a stochastic differential equation

$$\frac{d\eta}{dt} = F(\eta) + \xi(t), \quad \langle \xi(t)\xi(t')\rangle = \mathcal{A}\delta(t - t'). \tag{18}$$

For temporal white noise, the associated one-loop field-theoretic potential $\mathcal{V}$, Eq. (4), has been calculated in $d = 0$ dimensions in [31] and is given by (we set $\eta_0 = 0$)

$$\mathcal{V}[\eta] = \frac{1}{2}F^2(\eta) + \frac{1}{2}\mathcal{A}\{\mathrm{Re}\sqrt{[F'(\eta)]^2 + F(\eta)F''(\eta)} - \sqrt{[F'(\eta)]^2}\} + O(\mathcal{A}^2), \tag{19}$$

where Re indicates taking the real part of the expression. From this $\mathcal{V}$, we then calculate the one-loop effective force $F_{\mathcal{A}}(\eta) = (2\mathcal{V})^{1/2}$ [31] which is given by

$$F_{\mathcal{A}}(\eta) = F(\eta) + \frac{1}{2}\frac{\mathcal{A}}{F(\eta)}\{\mathrm{Re}\sqrt{[F'(\eta)]^2 + F(\eta)F''(\eta)} - \sqrt{[F'(\eta)]^2}\} + O(\mathcal{A}^2). \tag{20}$$

We remark in passing that, as discussed in [31], the original stochastic differential equation Eq. (18) can be written as an ordinary differential equation in terms of the effective noise-corrected force $F_{\mathcal{A}}$ as follows:

$$\frac{d\eta}{dt} = F_{\mathcal{A}}(\eta). \tag{21}$$

It is convenient to proceed by first establishing the constraints implied by the reality projector. For $r = 0$, Eq. (12) implies the tree-level force $F(\eta) = b\eta(1 - \eta^2)$. Then the expression under the first square root in Eq. (20) is $[F'(\eta)]^2 + F(\eta)F''(\eta) = b^2(1 - 12\eta^2 + 15\eta^4)$. This is *negative* on the open intervals $(-0.84, -0.31)$ and $(0.31, 0.84)$, zero on their end points, and is strictly positive elsewhere [38].

The one-loop effective potential is therefore given by

$$V_{\mathcal{A}}(\eta) = -\int F_{\mathcal{A}}(\eta)d\eta + v_1, \tag{22}$$

where v_1 is an integration constant. We define

$$\mathcal{I}_1 = \int \frac{d\eta}{F(\eta)} \sqrt{[F'(\eta)]^2 + F(\eta)F''(\eta)}. \tag{23}$$

This integral is evaluated in the Appendix and setting $\lambda=0$ in Eq. (A3) yields

$$2\mathcal{I}_1 = -\ln\left|\frac{2\sqrt{R}-12\eta^2+2}{\eta^2}\right| + 2\ln\left|\frac{4\sqrt{R}+18(\eta^2-1)+8}{\eta^2-1}\right| - \sqrt{15}\ln|2\sqrt{15R}+30\eta^2-12|, \tag{24}$$

valid whenever $R=1-12\eta^2+15\eta^4 \geq 0$. Otherwise, from Re in Eq. (20) we have $\mathcal{I}_1=0$. Next, we define $\mathcal{I}_2$ as follows:

$$\mathcal{I}_2 = \int \frac{d\eta}{F(\eta)} \sqrt{[F'(\eta)]^2}. \tag{25}$$

Since the function $\sqrt{[F'(\eta)]^2}=b|(1-3\eta^2)|$, then setting $\lambda=0$ in Eq. (A5) yields $\mathcal{I}_2$ which is

$$= \begin{cases} \frac{1}{2}\ln|\eta^2| + \ln|1-\eta^2| + c_1, & \left(-\frac{1}{\sqrt{3}} < \eta < \frac{1}{\sqrt{3}}\right) \\ -\frac{1}{2}\ln|\eta^2| - \ln|1-\eta^2| + c_2, & \left(\eta \leq -\frac{1}{\sqrt{3}} \,\&\, \frac{1}{\sqrt{3}} \leq \eta\right). \end{cases} \tag{26}$$

Matching up at $\eta^2=\frac{1}{3}$ ensures continuity in $\mathcal{I}_2$. Without loss of generality, we take $c_2=0$. Then $c_1=-\ln\frac{1}{3}-2\ln\frac{2}{3}\simeq 1.91$.

The effective potential Eq. (22) can be expressed in terms of the difference of these two integrals as follows:

$$V_{\mathcal{A}}(\eta) = V(\eta) - \frac{\mathcal{A}}{2}\{\mathcal{I}_1 - \mathcal{I}_2\} + O(\mathcal{A}^2), \tag{27}$$

up to constants of integration used to match up the one-loop corrections to ensure continuity. For domains over which $R \geq 0$, namely, $\eta<-0.84$, and $-0.31<\eta<0.31$ and $\eta>0.84$, then $\mathcal{I}_1$ is given by Eq. (24), otherwise when $R<0$, then $\mathcal{I}_1=0$. Thus, for those regions over which $R<0$, the one-loop correction in Eq. (27) is equal to $+\frac{\mathcal{A}}{2}\mathcal{I}_2$. On the two outer intervals $(-1,-0.84)$ and $(0.84,1)$, the one-loop correction is given by $-\frac{\mathcal{A}}{2}\{\mathcal{I}_1-\mathcal{I}_2\}$. From Eqs. (24) and (26), we calculate this quantity valid over these intervals and find that

$$\{\mathcal{I}_1 - \mathcal{I}_2\} = -\frac{1}{2}\ln\left|\frac{2\sqrt{R}-12\eta^2+2}{\eta^2}\right| + \frac{1}{2}\ln|\eta^2| + \ln|4\sqrt{R} + 18(\eta^2-1)+8| - \frac{\sqrt{15}}{2}\ln|2\sqrt{15R}+30\eta^2-12|. \tag{28}$$

Whereas for the central interval $(-0.31,0.31)$, we calculate this difference and find

$$\{\mathcal{I}_1 - \mathcal{I}_2\} = -\frac{1}{2}\ln|2\sqrt{R}-12\eta^2+2| - \ln|1-\eta^2| - c_1 + \ln\left|\frac{4\sqrt{R}+18(\eta^2-1)+8}{\eta^2-1}\right| - \frac{\sqrt{15}}{2}\ln|2\sqrt{15R} + 30\eta^2 - 12|. \tag{29}$$

Lastly, write $V_{\mathcal{A}}=V+(\mathcal{A}/2)\Delta V$ then the form of the pure one-loop correction $\Delta V(\eta)$ is completely specified as follows:

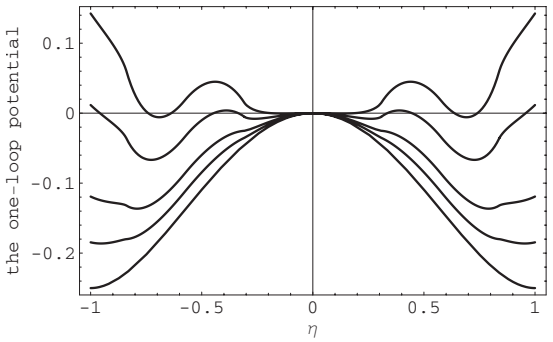

FIG. 4. The one-loop effective potential $V_{\mathcal{A}}/b$ for the Frank model, Eq. (27). The final enantiomeric excess η corresponds to the absolute minima of the potential and decreases in absolute value below unity as the noise strength increases. The curves from bottom to top correspond to $\mathcal{A}/2b=0.0$, 0.05, 0.1, 0.2, and 0.3.

$$\Delta V(\eta) = \begin{cases} \delta V_{out}(\eta) + v_1: & (-1,-0.84) \\ \mathcal{I}_2(\eta) + v_2: & (-0.84,-0.31) \\ \delta V_{in}(\eta) + v_3: & (-0.31,0.31) \\ \mathcal{I}_2(\eta) + v_2: & (0.31,0.84) \\ \delta V_{out}(\eta) + v_1: & (0.84,1). \end{cases}$$

Here, $-\delta V_{out}$ is given by Eq. (28), $-\delta V_{in}$ by Eq. (29), and $\mathcal{I}_2$ by Eq. (26). Matching up at the end points of the above subintervals fixes the constants $v_2=v_1+3.182$, $v_3=v_1-0.001$, where v_1 is an overall integration constant we are free to choose [see Eq. (22)]. We take $v_1=\delta V_{in}(0)$.

We now consider the role of weak external noise on mirror-symmetry breaking using the effective potential [39]. We first scale out by the factor b and evaluate $V_{\mathcal{A}}/b$ while varying the dimensionless noise amplitude $0 \leq \frac{\mathcal{A}}{2b} \ll 1$. The absolute minima of the effective potential correspond to the allowed stable final chemical states. From the sequence of curves in Fig. 4, corresponding to $\frac{\mathcal{A}}{2b}=0.0$, 0.05, 0.1, 0.2, and 0.3, we see that increasing the noise amplitude tends to destabilize the system. The homochiral states $|\eta|=1$ exist only in the absence of noise (see bottommost curve). For low levels of noise, the system has stable chiral states corresponding to $|\eta|<1$. The noise erodes the enantiomeric excess, driving it to absolute values less than unity.

A symmetric pair of new relative maxima begins to form and persist for $\mathcal{A}/2b \gtrsim \mathcal{A}_c/2b \simeq 0.2$, thus leading to a pair of seemingly metastable chiral states (see Fig. 4). At the same time, the potential's origin becomes locally flat and then curves upward to a local minimum for increasing noise levels. However, since Eq. (18) is a zero-dimensional system, we do not expect a true phase transition to occur as the noise intensity is increased. Instead, an increase in the noise serves to disorder the system and this is reflected in the shift of the relative minima $|\eta|<1$ which decrease continuously from unity as $\mathcal{A}/2b$ is increased from zero. Unlike the sequence of curves in Fig. 1, the pair of chiral minimum does not continuously approach and merge at the origin if the noise level is turned up. Independent evidence corroborating this behavior is provided by a Fokker-Planck equation analysis of the Landau model, which is mathematically similar to the system

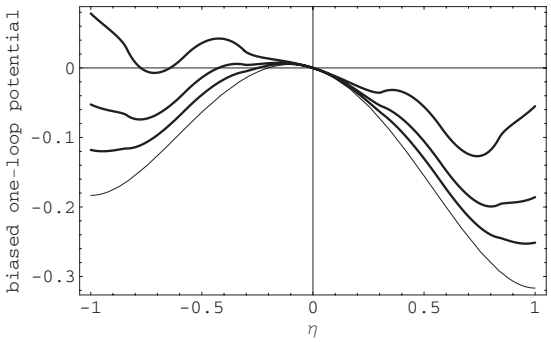

FIG. 5. The biased one-loop effective potential $V_{\mathcal{A}}/b$ for the Frank model with $\epsilon'=0.1$. The sequence of curves from bottom to top corresponds to $\mathcal{A}/2b=0.0$, 0.05,0.1, and 0.2. Compare and contrast to Fig. 4.

Eq. (18) considered here. In the Landau model, the noise-averaged order parameter $\langle|\eta|\rangle$ and its variance $\sigma=(\langle\eta^2\rangle-\langle|\eta|\rangle^2)/\mathcal{A}$ are calculated as functions of the noise intensity by means of the probability distribution function. The order parameter shows a decrease from unity as the noise is switched on that bottoms out at $\langle|\eta|\rangle_{minimum}\approx 0.8$ for $\mathcal{A}\approx 0.3$ and then rises very slowly as the noise is increased, but never approaches unity. The variance reaches a global maximum $\sigma\approx 0.8$ for $\mathcal{A}\approx 0.12$ followed by a monotone decrease for stronger levels of noise [40]. This behavior is regarded as indicating a noise-induced disordering transition.

Recall that our calculation of the potential Eq. (27) is founded on lowest-order perturbation theory and so is valid strictly for small noise intensities. We estimate an approximate critical intensity $\mathcal{A}_c/2b\simeq 0.3$ as the upper limit for which the one-loop approximation is likely to break down, since this is where the racemic state becomes a global minimum of the potential (see Fig. 4). That is, for noise intensities near or greater than this level, the potential would predict a discontinuous transition from a chiral to a racemic state, a feature not seen in the analysis of the Landau model discussed above. From the figure, we read off the minimum value of the enantiomeric excess to be approximately $|\eta|_{min}\approx 0.7$, which is in good agreement with the value obtained in the Landau model. Using the nominal values [18] $k_3\approx 10^2$ Ms^{-1}, $k_{-2}\approx 10^{-5}$ Ms^{-1}, and $\chi^*=1$ M, then $2b=100$ s^{-1}, we estimate external noises within the range $0\leq\mathcal{A}\lesssim 33$ s^{-1} would be perturbatively valid.

Finally, we consider the combined effect of noise and chiral bias. When we include noise, the one-loop biased effective potential is obtained by subtracting $\epsilon'(\eta-\eta^3/3)$ from the right-hand side of Eq. (27) and the overall expression is valid up to the second-order terms $O(\epsilon'\mathcal{A})$ and $O(\mathcal{A}^2)$. The effect of the bias is to tilt the noise-corrected potential in the same sense as shown in Fig. 3, so that the sequence of noise-induced minima located at $0<\eta\leq 1$ in Fig. 4 now becomes the *absolute* minimum (see Fig. 5). Due to this tilting, the origin of the potential is no longer locally flat, that is $V'_{\mathcal{A}}(0)\neq 0$ for any value of the noise. The noise has a destabilizing effect upon the biased system and the effective potential possesses a global minimum corresponding to a chiral but not homochiral state (see Fig. 5). The sense of tilt in the figure simply flips over for $\epsilon<0$. If the direct racemization step $L\leftrightarrow D$ is included in the Frank scheme Eqs. (6)–(8), then a recent numerical simulation suggests that additive noise can lead to enantioselection for otherwise tiny undetectable chiral biases [41].

IV. NOISE AND DIFFUSION IN TWO DIMENSIONS

Chemical reactions take place in space as well as in time. For well-mixed chemical systems, the condition we assumed in the previous section, then the spatial dependence plays no important role. In a well-mixed system, there are no concentration gradients and thus no *large-scale* diffusion. The well-mixed system is in effect zero dimensional. For poorly mixed or heterogeneous systems, spatial diffusion should be included and the associated effective potential, including the effects of a spatially dependent external noise, as in Eq. (2), can be calculated analytically within perturbation theory. Such an analytic expression for the square of the one-loop effective force $F_{\mathcal{A}}$ in reaction-diffusion equations subject to white noise has been calculated for arbitrary force terms F in $d=2$ dimensions in [31].

A. One-loop effective potential

To include the effects of diffusion, we replace $\frac{d}{dt}$ by $\frac{\partial}{\partial t}-D\nabla^2$ in Eq. (11), where D is the diffusion constant. As before, the simplest way to model a random environment is through additive white noise. So we next add spatially dependent external white noise $\xi(\boldsymbol{x},t)$ and then we have an SPDE of the form displayed in Eq. (1). In this case, the shape function $g_2(x-x')=\delta(\boldsymbol{x}-\boldsymbol{x}')\delta(t-t')$ and automatically satisfies Eq. (3). For $d=2$, the renormalized one-loop field-theoretic potential $\mathcal{V}$ in Eq. (4) is calculated in [31] and is given by

$$\mathcal{V}[\eta]=\frac{1}{2}F^2(\eta)+\frac{\mathcal{A}}{16\pi D}\left[F'(\sqrt{(F')^2+FF''}-\sqrt{(F')^2})-FF''\ln\left|\frac{\sqrt{(F')^2+FF''}-F'}{2D\mu^2}\right|+\frac{1}{2}FF''\right]+O(\mathcal{A}^2). \tag{30}$$

There is also a reality projector Re implicit in the derivation of this expression and we are instructed to take the real part [31]. The ratio $\frac{\mathcal{A}}{D}$ multiplying the one-loop term is dimensionless: thus we immediately appreciate that the relative magnitude of the correction term to the tree-level contribution is determined through the competing effects of noise and diffusion. Diffusion thus acts to "buffer" external disturbances. We also emphasize that the stochastic field theory for the SPDE Eq. (1) contains a hidden scale parameter $\mu\sim 1/l$, with units of an inverse length l, that must be introduced to define the parameters of the theory, that is, to *renormalize* it. In two dimensions, the expression Eq. (4) contains a logarithmic short-distance divergence which requires regularization and renormalization. The latter procedure introduces an arbitrary scale μ into the resultant expression. The dependence of the theory on this sliding scale parameter μ is described by the renormalization group and μ will appear in

the RG-improved effective potential. We will come back to this important point below.

The corresponding one-loop effective force implied by $\mathcal{V}$ is

$$F_{\mathcal{A}} = F + \frac{\mathcal{A}}{16\pi D}\left\{\frac{F'}{F}[\sqrt{(F')^2+FF''}-\sqrt{(F')^2}] - F''\ln\left|\frac{\sqrt{(F')^2+FF''}-F'}{2D\mu^2}\right| + \frac{1}{2}F''\right\} + O(\mathcal{A}^2). \tag{31}$$

Thus the effective mechanical potential corresponding to this force is given by

$$V_{\mathcal{A}} = -\int F_{\mathcal{A}}(\eta)d\eta + v_1. \tag{32}$$

Just as we did for the zero-dimensional case, we recall the subintervals over which the first square-root expression is real. For the moment consider $a=0$ and then the expression under the first square root in $F_{\mathcal{A}}$ can be written as

$$q = b^2(1-12\eta^2+15\eta^4). \tag{33}$$

This is *negative* on the intervals $(-0.84,-0.31)$ and $(0.31,0.84)$ and positive otherwise. For those intervals over which $q\geq 0$ the one-loop effective potential is given by

$$V_{\mathcal{A}}(\eta) = V(\eta) - \frac{\mathcal{A}}{16\pi D}\left\{\int d\eta\left(\frac{F'}{F}[\sqrt{(F')^2+FF''}-\sqrt{(F')^2}] - F''\ln\left|\frac{\sqrt{(F')^2+FF''}-F'}{2D\mu^2}\right| + \frac{1}{2}F''\right) + v_1\right\} + O(\mathcal{A}^2), \tag{34}$$

where v_1 is a constant of integration.

It is convenient to break the calculation down into smaller more manageable integrals. So, for $q\geq 0$, we define

$$\mathcal{I}_1 = \int d\eta\frac{F'(\eta)}{F(\eta)}\sqrt{[F'(\eta)]^2+F(\eta)F''(\eta)}, = \frac{b}{2}\int dx\left(\frac{1}{x}+\frac{2}{x-1}\right)\sqrt{1-12x+15x^2}, \tag{35}$$

where we have used the change of variables $x=\eta^2$ and the identity $\frac{1}{x(x-1)}=-\frac{1}{x}+\frac{1}{x-1}$.

We next define

$$\mathcal{I}_2 = \int d\eta\frac{F'(\eta)}{F(\eta)}\sqrt{[F'(\eta)]^2} = \frac{b}{2}\int dx\left(\frac{1}{x}+\frac{2}{x-1}\right)|1-3x|. \tag{36}$$

In close analogy with the prior $d=0$ effective potential calculation, we can combine these two integrals to determine their contribution $\{\mathcal{I}_1-\mathcal{I}_2\}$ over the full $-1\leq\eta\leq 1$ interval. First consider regions over which $R\geq 0$ and specifically the two outer intervals $(-1,-0.8399)$ and $(0.8399,1)$. From Eqs. (A3) and (A5) and setting $\lambda=3$, we calculate this difference and find

$$\{\mathcal{I}_1-\mathcal{I}_2\}/b = \frac{3}{2}\sqrt{R} - \frac{1}{2}\ln\left|\frac{2\sqrt{R}-12\eta^2+2}{\eta^2}\right| - 2\ln|4\sqrt{R} + 18(\eta^2-1)+8| + \frac{1}{2}\ln|\eta^2| + \frac{6}{\sqrt{15}}\ln|2\sqrt{15R} + 30\eta^2-12| - \frac{9}{2}\eta^2. \tag{37}$$

On the other hand, for the central interval $(-0.3074,0.3074)$, we calculate

$$\{\mathcal{I}_1-\mathcal{I}_2\}/b = \frac{3}{2}\sqrt{R} - \frac{1}{2}\ln|2\sqrt{R}-12\eta^2+2| - 2\ln\left|\frac{4\sqrt{R}+18(\eta^2-1)+8}{\eta^2-1}\right| + \frac{6}{\sqrt{15}}\ln|2\sqrt{15R} + 30\eta^2-12| + 2\ln|\eta^2-1| + \frac{9}{2}\eta^2 - c_1. \tag{38}$$

Next we define and calculate

$$\mathcal{I}_3 = \frac{1}{2}\int d\eta F''(\eta) = -\frac{3b}{2}\eta^2. \tag{39}$$

As for remaining integral, we also cast this in terms of the variable $x=\eta^2$,

$$\mathcal{I}_4 = \int d\eta F''\ln\left|\frac{\sqrt{(F')^2+FF''}-F'}{2D\mu^2}\right| = -6b\int d\eta\,\eta\ln\left|\frac{b(\sqrt{1-12\eta^2+15\eta^4}-(1-3\eta^2))}{2D\mu^2}\right|. \tag{40}$$

We employ an analytic approximation to this contribution as discussed in the Appendix [see Eqs. (A7) and (A8)].

We now have all the contributions to the one-loop correction. Then from Eq. (34), we can write

$$V_{\mathcal{A}}(\eta) = V(\eta) - \frac{\mathcal{A}}{16\pi D}[\{\mathcal{I}_1-\mathcal{I}_2\}+\mathcal{I}_3-\mathcal{I}_4] + O(\mathcal{A}^2) = V + \frac{\mathcal{A}}{16\pi D}\Delta V + O(\mathcal{A}^2),$$

$$\Delta V = -\{\mathcal{I}_1-\mathcal{I}_2\}-\mathcal{I}_3+\mathcal{I}_4, \tag{41}$$

and the form of the pure one-loop correction $\Delta V(\eta)$ is completely specified as follows in terms of the subinterval contributions

$$\Delta V(\eta) = \begin{cases} \delta V_{out}(\eta) - \mathcal{I}_3 + \mathcal{I}_4 + v_1: & (-1,-0.84) \\ \mathcal{I}_2(\eta) - \mathcal{I}_3 + \mathcal{I}_4 + v_2: & (-0.84,-0.31) \\ \delta V_{in}(\eta) - \mathcal{I}_3 + \mathcal{I}_4 + v_3: & (-0.31,0.31) \\ \mathcal{I}_2(\eta) - \mathcal{I}_3 + \mathcal{I}_4 + v_2: & (0.31,0.84) \\ \delta V_{out}(\eta) - \mathcal{I}_3 + \mathcal{I}_4 + v_1: & (0.84,1). \end{cases}$$

Here, $-\delta V_{out}$ is given by Eq. (37), $-\delta V_{in}$ by Eq. (38), and $\mathcal{I}_2$ by Eq. (A5). We match the individual contributions to the one-loop potential over the indicated subintervals. Once this is done, we can then assess the effects of diffusion and noise by varying the ratio $0 \leq \frac{\mathcal{A}}{16\pi D} \ll 1$. Before doing so, we must first turn to the renormalization-group equations (RGEs) to determine the μ-scale dependence of the model parameters (the various combinations of the reactions rates and chemical concentrations). This step will be required in order to carry out the perturbative RG improvement of the effective potential, which is the subject of the next section.

B. Renormalization group equations and improved potential

As we remarked above, the field-theoretic potential in $d=2$ dimensions has a short-distance logarithmic divergence which requires regularization and renormalization. These preliminary procedures were already carried out in [31] and this required introducing the arbitrary renormalization scale μ. The bare unrenormalized field-theoretic potential $\mathcal{V}$ Eq. (4) does not of course depend on the arbitrary renormalization scale μ so that we have the condition [31,42,43]

$$\mu \frac{d\mathcal{V}[\eta;d=2]}{d\mu} = 0. \tag{42}$$

This fact directly implies the following condition on the renormalized force [31]:

$$\mu \frac{dF(\eta)}{d\mu} = -\frac{\mathcal{A}}{8\pi D} F''(\eta) + O(\mathcal{A}^2). \tag{43}$$

We go back to the renormalized tree-level force and write it as follows, where $a(\mu)$ and $b(\mu)$ denote the renormalized parameters:

$$F(\eta) = -b(\mu)\eta^3 + [b(\mu) - 2a(\mu)]\eta,$$

$$F''(\eta) = -6b(\mu)\eta. \tag{44}$$

We insert these expressions back into the RGE Eq. (43), use the general theorem of algebra, and find that a and b must individually satisfy the following equations:

$$\mu \frac{db(\mu)}{d\mu} = 0 + O(\mathcal{A}^2), \tag{45}$$

$$\mu \frac{da(\mu)}{d\mu} = -\frac{3\mathcal{A}}{8\pi D} b(\mu) + O(\mathcal{A}^2). \tag{46}$$

Although b does not run with scale at one-loop order, a does run with the scale according to

$$a(\mu) = -\frac{3\mathcal{A}b}{8\pi D} \ln\left(\frac{\mu}{\mu_0}\right) + a(\mu_0) + O(\mathcal{A}^2), \tag{47}$$

where μ_0 is an initial scale (proportional to an initial inverse length scale $1/l_0$). Recall the discussion in Sec. II A of the racemizing tendency as $r=a/b \to 1/2$ in the tree-level potential. As we will demonstrate below, in the renormalization-group improved effective potential, the noise intensity and the running scale $\mu < \mu_0$ (i.e., the large length scale limit) in tandem induce a positive increase in r and thus tend to racemize the system.

A few words devoted to this procedure in Eqs. (43)–(47) are in order. RG improvement consists of substituting the bare parameters appearing in a field theory by their running, scale-dependent forms, calculated to some order in perturbation theory: e.g., here we replace $a, b \to a(\mu), b(\mu)$. The very scale dependence of these couplings or parameters is of course a consequence of the noise and fluctuations present in the theory. The scale dependence is handled by the renormalization group whose aim is to describe how the dynamics of a system evolves as we change the scale at which the phenomena are being observed. Improved perturbation theory then results from combining the tools of the RG with perturbation theory and allows us to go beyond the strict limitations imposed by conventional perturbation theory alone [42,43].

So, with the scale dependence of the parameters determined, to proceed, we insert $a(\mu)$ and $b(\mu)$ into the tree-level potential thus

$$\frac{V(\eta)}{b} = \frac{\eta^4}{4} + \left(r(\mu) - \frac{1}{2}\right)\eta^2, \tag{48}$$

$$r(\mu) = r(\mu_0) - \frac{3\mathcal{A}}{8\pi D} \ln\left(\frac{\mu}{\mu_0}\right) + O(\mathcal{A}^2). \tag{49}$$

Then the complete one-loop potential can be evaluated, varying not only the noise intensity and the diffusion constant, but also the sliding scale μ. Note we can insert the bare values of a and b into the pure one-loop term ΔV and we choose $a(\mu_0)=0$, i.e., no direct monomer production. This is valid to the one-loop order at which we are working, as the renormalized parameters $a(\mu)$, $b(\mu)$ are themselves of order $\mathcal{A}$ and any corrections would then be of second order $O(\mathcal{A}^2)$. So taking into account Eqs. (48) and (49), we evaluate and plot below the complete one-loop RG-improved effective potential

$$V_{\mathcal{A}}(\eta) = V(\eta) - \frac{\mathcal{A}}{16\pi D}[\{\mathcal{I}_1 - \mathcal{I}_2\} + \mathcal{I}_3 - \mathcal{I}_4] + O(\mathcal{A}^2)$$

$$= V + \frac{\mathcal{A}}{16\pi D}\Delta V,$$

$$\Delta V = -\{\mathcal{I}_1 - \mathcal{I}_2\} - \mathcal{I}_3 + \mathcal{I}_4. \tag{50}$$

By inspection of $V_{\mathcal{A}}(\eta)$, we have three independent dimensionless ratios to consider, namely, $\frac{\mathcal{A}}{16\pi D}$, the dimensionless noise intensity or loop-parameter plus $\frac{\mu}{\mu_0}$ as well as $\frac{|b|}{2D\mu^2}$. We

now establish their physical ranges and interpret them accordingly. The first one is fairly obvious, as we are dealing with perturbation theory so we should restrict $0 \leq \frac{\mathcal{A}}{16\pi D} \ll 1$. The actual magnitude of the perturbation depends on the relative strength of the external noise to the internal diffusion. Second, as there are no negative rate constants in chemistry, we must have $a(\mu) \geq 0$, which from Eq. (47), holds if and only if $\mu \leq \mu_0$ given that $b > 0$, the latter being the necessary condition for mirror-symmetry breaking. But this makes good physical sense since we are actually interested in the *large* length scale properties of the potential, which correspond to the limit $\mu \sim 1/l \to 0$. As remarked above, we set $a(\mu_0)=0$, which is equivalent to shutting off the direct monomer production step at the microlength scale $l_0 \sim 1/\mu_0$ of the chemical reactions. Lastly, the ratio $\frac{|b|}{2D\mu^2}$ can in principle be either greater or less than unity and we consider both of these possibilities below. In summary, the three independent ratios that define the effective large scale properties of the model are

$$0 \leq \frac{\mathcal{A}}{16\pi D} \ll 1, \quad 0 < \frac{\mu}{\mu_0} \leq 1, \tag{51}$$

$$0 < \frac{|b|}{2D\mu^2} \equiv \frac{\mu_{diff}^2}{\mu^2}, \tag{52}$$

where the latter ratio introduces an inverse length scale $\mu_{diff} = \frac{b}{2D}$ associated with the diffusion. Given the identification of $\mu_0 \sim 1/l_0$ as an initial inverse microlength scale, there are in principle four cases we can distinguish:

$$\begin{aligned} &\text{(I)}: \mu_{diff} = \mu_0 \\ &\text{(II)}: \mu_{diff} < \mu < \mu_0 \\ &\text{(III)}: \mu < \mu_{diff} < \mu_0 \\ &\text{(IV)}: \mu_{diff} \equiv \mu < \mu_0. \end{aligned} \tag{53}$$

This latter case translates into (IV): $\mu^2 = \frac{b}{2D}$, with $\mu < \mu_0$. So, this corresponds to identifying the sliding scale μ to the (inverse) diffusion length scale and the diffusion length scale *greater* than the microscopic length scale. This is physically reasonable. From this perspective, the cases (II) and (III) allow for the diffusion length scale to be greater or lesser than the sliding length scale, but both of these are individually greater that the microlength scale and we will see below there is no essential difference between any of the three latter cases. There is, however, a major qualitative difference between these cases and case (I).

C. Chiral symmetry restoration and racemization

To further drive home the significance of the relative length scales involved, we estimate some characteristic values of the diffusion length scale $l_{diff} \sim 1/\mu_{diff}$ associated with molecular diffusion in water at room temperature, as well as length scales typical of the turbulent eddy diffusivities as actually measured in the ocean [44]. Such large scale flows were argued to be relevant for the spreading of homochirality in the ocean [22]. It will be clear that l_{diff} is indeed a macroscopic length scale.

The molecular diffusion in water (at room temp) is

$$D = 10^{-9} \ \text{m}^2/\text{s}.$$

Turbulent (eddy) diffusivity in the ocean is

$$D \simeq 10^{-4} \ \text{m}^2/\text{s} \quad \text{(vertical-mixing)}$$

and

$$D \simeq 10^{3} \ \text{m}^2/\text{s} \quad \text{(horizontal-mixing)}.$$

Then using the nominal values $k_3 = 10,100$ M/s [18] and $\chi^* = 1$ M, the characteristic reaction time scales are given by

$$b = 5 \ \text{s}^{-1}, \ 50 \ \text{s}^{-1}.$$

The associated diffusion length scales are as follows:

Diffusion length scale (water)

$$l_{diff} = \left(\frac{2D}{b}\right)^{1/2} = \left(\frac{2 \times 10^{-9} \ \text{m}^2/\text{s}}{5 \ \text{s}^{-1}}\right)^{1/2} = 2 \times 10^{-5} \ \text{m} = 2 \times 10^{-3} \ \text{cm}. \tag{54}$$

Diffusion length scale (vertical eddy diffusivity)

$$l_{diff} = \left(\frac{2D}{b}\right)^{1/2} = \left(\frac{2 \times 10^{-4} \ \text{m}^2/\text{s}}{5 \ \text{s}^{-1}}\right)^{1/2} = 0.63 \times 10^{-2} \ \text{m} = 0.63 \ \text{cm}. \tag{55}$$

Diffusion length scale (horizontal eddy diffusivity)

$$l_{diff} = \left(\frac{2D}{b}\right)^{1/2} = \left(\frac{2 \times 10^{3} \ \text{m}^2/\text{s}}{5 \ \text{s}^{-1}}\right)^{1/2} = 20 \ \text{m} = 2000 \ \text{cm}. \tag{56}$$

Choosing the second estimate for b above just decreases the diffusion length scales by an overall factor of 10.

With this intended to orient the physical context, we turn to the evaluation of the RG-improved effective potential for the various cases listed above in Sec. IV B. Identifying the relative scales as per case I, we have

$$\mu_0^2 = \frac{|b|}{2D} \Rightarrow \frac{|b|}{2D\mu^2} = \frac{\mu_0^2}{\mu^2}. \tag{57}$$

This case is somewhat *outré* in that we are identifying the macro- and microscopic length scales: $l_{diff} = l_0$. This results in an exact cancellation between the logarithm term in the renormalized tree potential, Eqs. (48) and (49), and the logarithm in the $\mathcal{I}_4$ integral contribution, Eq. (40). The dependence on the sliding scale μ thus drops out of the expression for the one-loop potential Eq. (50) and the only remaining free parameter is the ratio of the noise intensity to the diffusion. We evaluate Eq. (50) for various values of the noise parameter as shown Fig. 6. For zero noise intensity, we recover the classic double-well potential indicating that the final chemical states will be homochiral $\eta = \pm 1$ with equal probability (see bottom curve). At this microlength scale l_0, for increasing noise intensity, we observe that the potential minima deepen at $\eta = \pm 1$ while the origin $\eta = 0$ changes

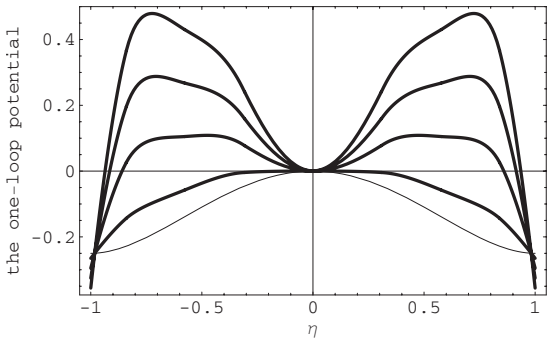

FIG. 6. (Case I) With $\mu_{diff}=\mu_0$. The $d=2$ one-loop effective potential $V_{\mathcal{A}}/b$ for the Frank model. The μ dependence drops out in this case. The range of the noise parameter $\frac{\mathcal{A}}{16\pi D}=(0,0.1,0.3,0.5,0.7)$ corresponds to the sequence of curves from bottom to top.

from being a global maximum (negatively curved) to a local minimum (positively curved), indicating that the racemic state goes from being a completely unstable state to a metastable state. Note however that a high potential barrier separates the racemic from the chiral states at this smaller length scale.

When the diffusion length scale is greater than the initial scale $l_{diff}>l_0$, then we are in the regime of cases II–IV, which are all qualitatively very similar. In Fig. 7, we plot the potential for case II for $l_{diff}=10\times l_0$ and $l=5\times l_0$ and for a range of reasonably small noise intensities.

Here the situation is strikingly distinct from that of case I. When the diffusion length scale is greater than the initial microscale, then the noise induces a true phase transition, whereby the stable homochiral states that pertain in the absence of any noise are destabilized and the racemic state emerges as the unique stable outcome for noise intensities above a certain critical value; compare to Fig. 6. There is a continuous merger of the two chiral minima at the origin as the noise intensity increases, a characteristic typical of second-order transitions.

For $\mu<\mu_{diff}<\mu_0$, we have case III. This means the scale of observation $l>l_{diff}$ is greater than the diffusion length scale and both are larger than the initial scale l_0. This is plotted in Fig. 8 for $l_{diff}=5\times l_0$ and $l=10\times l_0$ and a range of

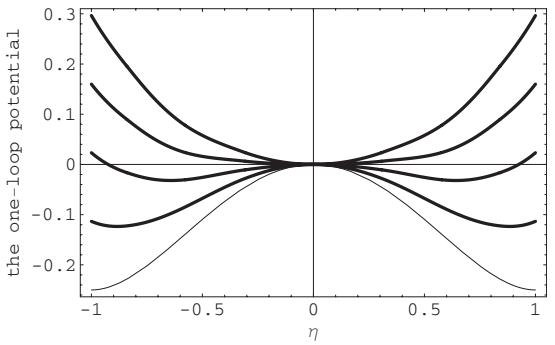

FIG. 7. (Case II) The $d=2$ one-loop effective potential $V_{\mathcal{A}}/b$. With $\mu_{diff}\leq\mu<\mu_0$, specifically: $l_{diff}=10\times l_0$, and $l=5\times l_0$. Noise parameter $\frac{\mathcal{A}}{16\pi D}=(0,0.01,0.02,0.03,0.04)$; sequence of curves from bottom to top.

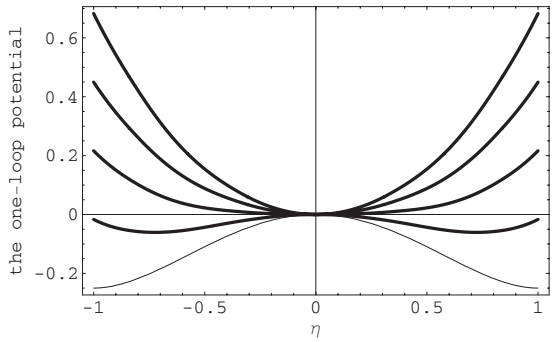

FIG. 8. (Case III) The $d=2$ one-loop effective potential $V_{\mathcal{A}}/b$. With $\mu<\mu_{diff}<\mu_0$. Specifically, $l_{diff}=5\times l_0$ and $l=10\times l_0$. Noise parameter $\frac{\mathcal{A}}{16\pi D}=(0,0.01,0.02,0.03,0.04)$; sequence of curves from bottom to top.

small noise intensities. The potential is qualitatively similar to that of case II (compare to Fig. 7).

Finally, for $\mu=\mu_{diff}<\mu_0$, we have case IV. The scale of observation $l=l_{diff}$ is identical to the diffusion length scale and larger than the initial length scale l_0. This situation is plotted in Fig. 9 for $l_{diff}=1000\times l_0$ and for a range of small noise intensities. We also considered the alternative choices $l_{diff}=10\times l_0$ and $l_{diff}=100\times l_0$, but these yield no qualitative differences in the form of the effective potential.

As remarked above, we confirm that there are only two qualitatively distinguishable cases. Namely, case I stands apart from cases II–IV. That is, either we are "sitting right on top" of the initial chemical microscale $\mu_{diff}=\mu_0$, in which case the chiral states are still the most stable, even when noise is turned on (the racemic state becomes metastable), or else we are observing the system at length scales $\mu_{diff}<\mu_0$ and $\mu<\mu_0$ larger than this chemical microscale, for which increasing noise has a *bona fide* racemizing tendency leading to a phase transition: increasing the noise level drives the two equivalent chiral minima to the origin in a continuous fashion. We did not observe this transition behavior in zero dimensions $d=0$, for which we detect only a noise-induced destabilizing effect, but no true phase transition.

From Fig. 9 and for the relative scales involved there, we may roughly estimate the critical value of the loop parameter to be $\frac{\mathcal{A}}{16\pi D}\approx 0.015$. On the other hand, the purely numerical simulations in $d=2$ reported in the first two papers of [27]

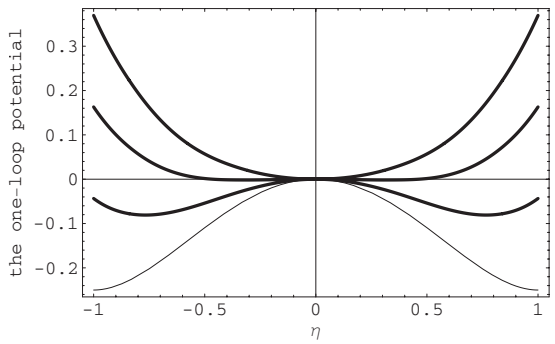

FIG. 9. (Case IV) The $d=2$ one-loop effective potential $V_{\mathcal{A}}/b$. With $\mu=\mu_{diff}$ and $l_{diff}=1000\times l_0$. Noise parameter $\frac{\mathcal{A}}{16\pi D}=(0,0.005,0.01,0.015)$; sequence of curves from bottom to top.

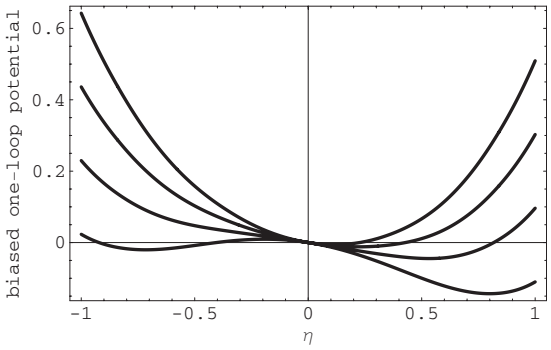

FIG. 10. The biased $d=2$ one-loop effective potential $V_{\mathcal{A}}/b$ for $\epsilon'=0.1$ and $\mu=\mu_{diff}$ and $l_{diff}=1000\times l_0$. Noise parameter $\frac{\mathcal{A}}{16\pi D}=(0.005, 0.01, 0.015, 0.02)$; sequence of curves from bottom to top.

yield $\frac{\mathcal{A}_c}{D}\simeq 1.15$ for a computation over an $L\times L$ domain where $L=1024\delta x$ and δx is the lattice spacing. We tentatively identify L with l_{diff} and δx with the microlength scale l_0. Dividing the simulated value of the critical noise parameter by the geometric factor $16\pi\simeq 50$ yields $(\frac{\mathcal{A}_c}{16\pi D})_{\text{Gleiser}}\approx 1.15/50=0.023$ in $d=2$. Bearing in mind that the model treated by Gleiser and co-workers is an $N=2$ truncation of Sandar's polymerization reaction network, we regard this as a rather good agreement between the analytic calculation carried out here and the direct numerical simulation reported in [27].

D. Chiral bias plus noise

We consider the combined effect of chiral bias and spatial noise in $d=2$ dimensions by subtracting the terms $\epsilon'(\eta-\frac{\eta^3}{3})$ from the right-hand side of $V_{\mathcal{A}}$ in Eq. (50), which will be valid up to the second-order terms $O(\epsilon'\mathcal{A})$ and $O(\mathcal{A}^2)$. The effective potential is tilted and for increasing noise levels the resultant inequivalent pair of chiral minima merge continuously to the limiting *nonzero value* $\eta\simeq\epsilon'$, indicating that there is no racemization in the presence of bias. This is illustrated in Fig. 10, in which we include chiral bias to the situation defined in case IV. Of course, if the bias is very small, say less than the intrinsic statistical chiral imbalance [45], then it will not be detected. For example, $\epsilon=\frac{\Delta E}{kT}\approx 10^{-17}$ for parity violation in the electroweak interactions at room temperature, where ΔE is the energy difference between the two enantiomers [37], whereas the intrinsic statistical deviations about the ideal racemic composition are on the order of $|\eta|_{statistical}\simeq 6.7\times 10^{-9}\%$ for millimolar (laboratory-size) samples [45].

V. DISCUSSION

In this paper, we have applied the stochastic field-theory formalism in [30,31] to study the impact of external noise on chirality in a key model of SMSB. We focused on the elementary Frank model due to the central role it plays in theoretical approaches to mirror-symmetry breaking [9,11,12,18,19,21–24,27,28,34–37,39]. By purely analytic means, we verified that weak noise tends to racemize the system, eroding homochirality. In zero-dimensional or well-mixed systems, the noise disorders the system and there is no transition to a racemic state. By contrast, in two space dimensions with diffusion, the system does undergo a continuous phase transition to a racemic state. We obtain this result from renormalization-group improving the potential [42,43] to one-loop order in perturbation theory. At length scales above the microscale cutoff of the chemical reactions themselves, increasing noise levels drive the potential minima from chiral to racemic states in a continuous fashion. Since the chiral to racemic transitions examined here all occur for loop parameters $\frac{\mathcal{A}}{16\pi D}$ all lying in the range from 10^{-3} to 10^{-2}, we regard this as valid results within the limits of perturbation theory and confirms previous direct numerical results obtained by Gleiser and co-workers [27].

An important feature of this approach is the μ-scale dependence of the RG-improved effective potential $V_{\mathcal{A}}$ in $d=2$ dimensions. Because the field-theory potential $\mathcal{V}$ requires *renormalization*, the Frank model parameters necessarily run with scale and the racemizing tendency of the noise is therefore a weakly scale-dependent phenomena. We established that two qualitatively distinct cases arise as a result, namely, (i) when one observes the system at the short length scales typical of the chemical reactions themselves or (ii) when the system is observed at the larger length scales typical of molecular diffusion. For the former, the chiral states are still the most stable outcome, regardless of how strong the noise may be, whereas for the latter, the racemic state will be the unique stable outcome for noise levels exceeding a critical value. This scale dependence is in keeping with the aim or purpose of the renormalization group, which is to "describe how the dynamics of a system evolves as one changes the scale of the phenomena being observed" [46]. Since we are interested in the large length scale properties of the system, the latter case (ii) is the most interesting one. The dependence of chirality on length scale can be appreciated visually through direct numerical simulations in two dimensions. At small scales, the reaction domain is typically composed of a myriad of tiny chiral domains, but when averaged (course-grained) over the entire domain, the overall configuration can be close to racemic [22,28].

We have considered effects due to external noise. Other independent sources of randomness are present in reacting systems and it is important to carefully distinguish internal from external noises. One is at liberty to couple the reacting system to any external random force of one's choosing, the temporal and/or spatial dependence is not determined by the critical state of the chemical system; it is after all, external and is not slaved to the internal state of the chemical system. If the system is near a bifurcation point, then small amplitude external noise can have important effects as we have demonstrated here.

By contrast, internal noise depends on the state of the chemical system and one is not free to choose its mathematical form. There are two kinds of internal noise at play: (i) statistical and (ii) reaction noise. The former arises because exactly equal proportions of the two chiral enantiomers never occur in practice and this inevitable chiral imbalance yields an initial statistical enantiomeric excess [45]. In the latter, diffusion-limited noise is always present to some degree in imperfectly mixed spatially heterogeneous systems

and is sufficient to drive the mirror-symmetry breaking [28,34].

ACKNOWLEDGMENTS

We are grateful to Professor Josep M. Ribó for ongoing and informative discussions about mirror-symmetry breaking. This research is supported in part by Grant No. AYA2006-15648-C02-02 from the Ministerio de Educación y Ciencia (Spain) and forms part of the COST Action CM07030: *Systems Chemistry*.

APPENDIX: SOME INTEGRALS

Here we list the individual integrals needed to evaluate the pure one-loop corrections to the potential ΔV in both $d=0$ and in $d=2$ space dimensions. For $\mathrm{Re}\sqrt{[F'(\eta)]^2+F(\eta)F''(\eta)}>0$ we define

$$\mathcal{I}_1^\lambda = \frac{b}{2}\int dx \frac{(1-\lambda x)}{x(1-x)}\sqrt{1-12x+15x^2} \tag{A1}$$

$$= \frac{b}{2}\int dx\left(\frac{1}{x}+\frac{1-\lambda}{x-1}\right)\sqrt{1-12x+15x^2}, \tag{A2}$$

where $\lambda=0(\lambda=3)$ for $d=0(d=2)$, respectively. Then from [47], we have

$$\mathcal{I}_1^\lambda/b = \frac{\lambda}{2}\sqrt{R}+\frac{9\lambda-15}{2\sqrt{15}}\ln\left|2\sqrt{15R}+30x-12\right| - \frac{1}{2}\ln\left|\frac{2\sqrt{R}+2-12x}{x}\right| - (\lambda - 1)\ln\left|\frac{4\sqrt{R}+18(x-1)+8}{x-1}\right|. \tag{A3}$$

Otherwise $\mathcal{I}_1^\lambda=0$ when $\mathrm{Re}\sqrt{[F'(\eta)]^2+F(\eta)F''(\eta)}=0$.

Next, define

$$\mathcal{I}_2^\lambda = \frac{b}{2}\int dx\left(\frac{1}{x}+\frac{1-\lambda}{x-1}\right)|1-3x|, \tag{A4}$$

where again $\lambda=0(\lambda=3)$ for $d=0(d=2)$, respectively. Then $\mathcal{I}_2^\lambda/b$,

$$= \begin{cases} \frac{1}{2}\ln|\eta^2| + (1-\lambda)\ln|1-\eta^2| - \frac{3}{2}\eta^2 + c_1, & \text{for}\left(-\frac{1}{\sqrt{3}} < \eta < \frac{1}{\sqrt{3}}\right) \\ -\frac{1}{2}\ln|\eta^2| - (1-\lambda)\ln|1-\eta^2| + \frac{3}{2}\eta^2 + c_2, & \text{for}\left(\eta \le -\frac{1}{\sqrt{3}} \,\&\, \frac{1}{\sqrt{3}} \le \eta\right). \end{cases} \tag{A5}$$

Match these two pieces up at $\eta^2=1/3$. Without loss of generality, we take $c_2=0$. Then for $d=0$, $c_1=-\ln\frac{1}{3}-2\ln\frac{2}{3}\simeq 1.91$, whereas for $d=2$, then $c_1=-\ln\frac{1}{3}+4\ln\frac{2}{3}+3\simeq 2.477$.

Finally, we need to evaluate the integral $\mathcal{I}_4$. From Eq. (40) we can write

$$\mathcal{I}_4/b = -3\int dx\ \ln\left|\sqrt{1-12x+15x^2}-(1-3x)\right| - 3\int dx\ \ln|b/2D\mu^2|. \tag{A6}$$

The first integral however in Eq. (A6) cannot be worked out in closed form. It is also singular at the origin $x=0(\eta^2=0)$ so a further renormalization would be required to render the potential finite. We can take care of both of these problems by approximating the integral by one we can work out in closed form, namely,

$$\mathcal{J}_4/b = -3\int dx\ \ln\left|\sqrt{15}x-6/\sqrt{15}+\sqrt{15x^2-12x+1}\right|$$

$$= \frac{-3}{\sqrt{15}}\left[\left(\sqrt{15}\eta^2-\frac{6}{\sqrt{15}}\right)\ln\left|\sqrt{15}\eta^2-\frac{6}{\sqrt{15}}+\sqrt{R}\right| - \mathrm{Re}\sqrt{R}\right]. \tag{A7}$$

This means we will put

$$\mathcal{I}_4/b \to \mathcal{J}_4/b - 3\ln\left(\frac{|b|}{2D\mu^2}\right)\eta^2 \tag{A8}$$

into the expression for the one-loop correction ΔV to the potential, Eq. (41).

[1] P. Frank, W. A. Bonner, and R. N. Zare, in *Chemistry for the 21st Century*, edited by E. Keinan and I. Schecter (Wiley, Weinheim, 2000), p. 175.

[2] M. Avalos, R. Babiano, P. Cintas, J. L. Jimenez, J. C. Palacios, and L. D. Barron, Chem. Rev. (Washington, D.C.) **98**, 2391 (1998).

[3] J. Podlech, Angew. Chem., Int. Ed. **38**, 477 (1999); Cell. Mol. Life Sci. **58**, 44 (2001).

[4] I. Weissbuch, L. Leiserowitz, and M. Lahav, Top. Curr. Chem. **259**, 123 (2005).
[5] W. A. Bonner, Origins Life Evol. Biosphere **29**, 615 (1999).
[6] A. Guijarro and M. Yus, *The Origin of Chirality in the Molecules of Life* (RSC Publishing, Cambridge, 2009).
[7] S. Fox, J. Chem. Educ. **34**, 472 (1957).
[8] J. L. Bada and S. L. Miller, BioSystems **20**, 21 (1987).
[9] V. A. Avetisov, V. I. Goldanskii, and V. V. Kuzmin, Dokl. Akad. Nauk SSSR **282**, 115 (1985); V. I. Goldanskii, V. A. Avetisov, and V. V. Kuzmin, FEBS Lett. **207**, 181 (1986); V. Avetisov and V. Goldanskii, Proc. Natl. Acad. Sci. U.S.A. **93**, 11435 (1996).
[10] L. E. Orgel, Nature (London) **358**, 203 (1992).
[11] D. G. Blackmond, Proc. Natl. Acad. Sci. U.S.A. **101**, 5732 (2004).
[12] F. C. Frank, Biochim. Biophys. Acta **11**, 459 (1953).
[13] A. R. Hochstim, Origins Life **6**, 317 (1975).
[14] S. F. Mason, Nature (London) **314**, 400 (1985).
[15] S. F. Mason, *Chemical Evolution* (Oxford University Press, Oxford, 1991).
[16] K. D. Kondepudi and K. Asakura, Acc. Chem. Res. **34**, 946 (2001); K. Mikami and M. Yamanaka, Chem. Rev. (Washington, D.C.) **103**, 3369 (2003); R. Plasson, D. K. Kondepudi, H. Bersini, A. Commeyras, and K. Asakura, Chirality **19**, 589 (2007); R. Plasson, H. Bersini, and A. Commeyras, Proc. Natl. Acad. Sci. U.S.A. **101**, 16733 (2004).
[17] J. Rivera Islas, D. Lavabre, J.-M. Grevy, R. Hernández Lamoneda, H. Rojas Cabrera, J.-C. Micheau, and T. Buhse, Proc. Natl. Acad. Sci. U.S.A. **102**, 13743 (2005).
[18] J. Crusats, D. Hochberg, A. Moyano, and J. M. Ribó, ChemPhysChem **10**, 2123 (2009).
[19] I. Gutman, D. Todorović, and M. Vučković, Chem. Phys. Lett. **216**, 447 (1993).
[20] In this paper, the symbols "*L*" (left handed) and "*D*" (right handed) are used to refer only to the molecule's geometrical or spatial conformation. Handedness, or chirality, is an extrinsic property. Crystal chirality can be determined from its optical activity. However, and this is the subtle point to be aware of, some left-handed molecules rotate plane-polarized light in the clockwise sense, while others do so in the anticlockwise sense (and similarly for right-handed molecules). For this reason, we refrain from employing the terminology "levo" and "dextro," which refer strictly to the *intrinsic* optical properties of (chiral) molecules.
[21] P. G. H. Sandars, Origins Life Evol. Biosphere **33**, 575 (2003).
[22] A. Brandenburg and T. Multamäki, Int. J. Astrobiol. **3**, 209 (2004).
[23] J. A. Wattis and P. V. Coveney, Origins Life Evol. Biosphere **35**, 243 (2005).
[24] Y. Saito and H. Hyuga, J. Phys. Soc. Jpn. **74**, 1629 (2005).
[25] D. K. Kondepudi, R. J. Kaufman, and N. Singh, Science **250**, 975 (1990).
[26] C. Viedma, Phys. Rev. Lett. **94**, 065504 (2005).
[27] M. Gleiser and J. Thorarinson, Origins Life Evol. Biosphere **36**, 501 (2006); M. Gleiser, *ibid.* **37**, 235 (2006); M. Gleiser and S. I. Walker, *ibid.* **38**, 293 (2008); M. Gleiser, J. Thorarinson and S. I. Walker, *ibid.* **38**, 499 (2008).
[28] D. Hochberg and M.-P. Zorzano, Chem. Phys. Lett. **431**, 185 (2006).
[29] D. Todorović, I. Gutman, and M. Radulović, Chem. Phys. Lett. **372**, 464 (2003).
[30] D. Hochberg, C. Molina-París, J. Pérez-Mercader, and M. Visser, Phys. Rev. E **60**, 6343 (1999).
[31] D. Hochberg, C. Molina-París, J. Pérez-Mercader, and M. Visser, J. Stat. Phys. **99**, 903 (2000).
[32] S. Weinberg, *The Quantum Theory of Fields I and II* (Cambridge University Press, Cambridge, England, 1996).
[33] J. Zinn-Justin, *Quantum Field Theory and Critical Phenomena*, 4th ed. (Oxford University Press, Oxford, 2002).
[34] D. Hochberg and M.-P. Zorzano, Phys. Rev. E **76**, 021109 (2007).
[35] M. Avalos, R. Babiano, P. Cintas, J. L. Jimenez, and J. C. Palacios, Tetrahedron: Asymmetry **11**, 2845 (2000).
[36] I. Gutman, V. Babović, and S. Jokić, Chem. Phys. Lett. **144**, 187 (1988).
[37] D. K. Kondepudi and G. W. Nelson, Physica A **125**, 465 (1984).
[38] The exact endpoints are $\pm\{(6\pm\sqrt{21})/15\}^{1/2}$.
[39] D. Hochberg, Phys. Rev. Lett. **102**, 248101 (2009).
[40] J. García-Ojalvo and J. M. Sancho, *Noise in Spatially Extended Systems* (Springer, New York, 1999).
[41] J. M. Cruz, P. Parmananda, and T. Buhse, J. Phys. Chem. A Lett. **112**, 1673 (2008).
[42] M. E. Peskin and D. V. Schroeder, *An Introduction to Quantum Field Theory* (Westview Press, Boulder, 1995).
[43] D. Hochberg, C. Molina-París, J. Pérez-Mercader, and M. Visser, Int. J. Mod. Phys. A **14**, 1485 (1999).
[44] R. H. Stewart, *Introduction to Physical Oceanography* (2003), Chap. 8. http://oceanworld.tamu.edu/resources/ocng-textbook/contents.html
[45] W. H. Mills, Chem. Ind. (London) **10**, 750 (1932); K. Mislow, Collect. Czech. Chem. Commun. **68**, 849 (2003).
[46] D. Gross, in *Methods in Field Theory*, edited by R. Balian and J. Zinn-Justin (North-Holland, Amsterdam, 1981), pp. 141–250.
[47] H. B. Dwight, *Tables of Integrals and Other Mathematical Data*, 3rd ed. (The Macmillan Company, New York, 1957).